



HAL
open science

Fast oil-in-water emulsification in microchannel using head-on impinging configuration: Effect of swirl motion

Yongbin Ji, Jérôme Bellettre, Agnès Montillet, Patrizio Massoli

► **To cite this version:**

Yongbin Ji, Jérôme Bellettre, Agnès Montillet, Patrizio Massoli. Fast oil-in-water emulsification in microchannel using head-on impinging configuration: Effect of swirl motion. *International Journal of Multiphase Flow*, 2020, 131, pp.103402. 10.1016/j.ijmultiphaseflow.2020.103402 . hal-02924406

HAL Id: hal-02924406

<https://hal.science/hal-02924406>

Submitted on 26 Feb 2021

HAL is a multi-disciplinary open access archive for the deposit and dissemination of scientific research documents, whether they are published or not. The documents may come from teaching and research institutions in France or abroad, or from public or private research centers.

L'archive ouverte pluridisciplinaire **HAL**, est destinée au dépôt et à la diffusion de documents scientifiques de niveau recherche, publiés ou non, émanant des établissements d'enseignement et de recherche français ou étrangers, des laboratoires publics ou privés.

Impinging Configuration: Effect of Swirl Motion

Yongbin Ji ^a, Jérôme Bellettre ^{a,*}, Agnès Montillet ^b, Patrizio Massoli ^c^a LTeN UMR CNRS 6607, Université de Nantes, 1 rue Christian Pauc, CS 50609, 44306 Nantes Cedex 3, France^b GEPEA UMR CNRS 6144, Université de Nantes, 37 boulevard de l'Université, BP 406, 44602 Saint Nazaire, France^c Istituto Motori - CNR, Via Marconi 8, 80125 Napoli, Italy**Abstract**

Liquid-liquid dispersion by head-on impingement in a cross-slot microfluidic device to form oil-in-water emulsion is experimentally investigated at broad range of flow rate conditions. Reynolds number based on the continuous aqueous phase flow is changed from 1000 to 7000 and the oil dispersed volume fraction varies between 3% and 30%. The flow patterns are observed in the vicinity of impinging region to characterize the effect of Reynolds number and oil volume fraction on the water-oil interaction and thus emulsification process. Based on the measured droplet size and size distribution, two geometries are compared, aimed at evaluating the advantages and disadvantages of swirl flow in the collision region for producing high quality emulsion. One configuration, "600-600", corresponds to inlet channels of identical size ($600\ \mu\text{m} \times 600\ \mu\text{m}$), while the other one, "600-300", has a smaller channel for dispersed phase which is off-axis with the water channel. The results show that flow characteristics during dispersing process are significantly different for viscous and turbulent conditions. Dominated by Reynolds number, the flow patterns are classified into three regimes. The more turbulent the flow is, the finer and more monodispersed droplets will be in the o/w emulsion. In the medium Reynolds number regime, characteristics of flow are closer to laminar flow using higher oil volume fraction, compared to small oil volume content. It is particularly evident with 600-300 system because of lowering velocity gradient between two phase streams. Based on results of drop mean diameter and polydispersity index, 600-300 system which generates swirl flow structure only exhibits a superior performance, compared to the conventional equal-size geometry, at relatively higher Reynolds number.

Key words: oil-in-water emulsification; flow pattern, microfluidics, impingement, turbulent

Nomenclature

C	constant, -
D	diameter of the droplet, μm
\bar{D}	droplet mean diameter, μm
D_{10}	arithmetic mean diameter, μm
D_{32}	the Sauter mean diameter, μm
D_{max}	maximum droplet diameter, μm
f	oil volume fraction, -
G	velocity gradient, $1/\text{s}$
I	momentum flux, $\text{kg}/\text{m}\ \text{s}^2$
\dot{m}	mass flow rate, kg/s
P	pressure, bar
p_L	Laplace pressure, bar
Q	volume flow rate, mL/min
R	radius of the droplet, μm
U	superficial velocity, m/s
u_λ	velocity difference in the turbulent flow, m/s
V	volume, m^3

Greeks

γ	surface tension, mN/m
----------	---------------------------------------

δ	
ε	energy dissipation rate, W/kg
λ	turbulence eddy size, μm
λ_k	Kolmogorov length, μm
μ	dynamic viscosity, mPa s
ν	kinematic viscosity, m^2/s
ρ	density, kg/m^3
σ	interfacial tension, mN/m
τ_p	dynamic pressure fluctuation stress, bar
τ_s	shear stress, bar

Subscripts

c	continuous phase (water)
d	dispersed phase (oil)
e	emulsion

Acronyms

PdI	polydispersity index,-
Re	Reynolds number,-
We	Weber number,-

1. Introduction

Emulsification is a paramount technology widely carried out in foods (Galus and Kadzińska, 2015), pharmacy (Pouton, 1997), energy (Kokal, 2005; Kumar et al., 2009) industries and so on. Conceptually, it is realized by dispersing one phase liquid into another immiscible one with the assistance of various mixing methods. The emulsion quality (Shaw, 1980) indicated by the size of droplets and its distribution depends on the hydrodynamic condition of the emulsification device, as well as on the physical and interfacial properties of the two phases. From the perspective of various engineering applications, developing highly efficient facilities to continuously produce emulsion with defined size distribution of the dispersed phase is one of the major goals at present and in the future.

Extensive work has been devoted to study different methods of emulsification. The most conventional and common practice is to work in the batch mode, agitating the mixture of two-phase liquids in a tank using impellers or magnetic force (Chen and Middleman, 1967; Ohtake et al., 1987). Static mixers (Lemenand et al., 2003; Theron and Sauze, 2011) and high-pressure homogenizers (Schultz et al., 2004; Schlender et al., 2015) allow continuous operations but are less commonly used for industrial applications. Membrane emulsification (Joscelye and Trägårdh, 2000; Nakashima et al., 2000) is also proposed and investigated; however, in practice many technical locks such as fouling make that this kind of process is not extensively developed in the industry so far. Habchi et al. (2009) and Lemenand et al. (2014) studied mixing by chaotic advection in a special designed twisted-pipe flow for the water/oil dispersions generation process. It is concluded that shear stress is enhanced because of inducing secondary flow in the twisted-pipe compared with the straight-pipe flow, thus resulting dispersions are finer and more mono-dispersed. Another important technical branch, microfluidics, attracts plenty of focus these last decades. Use of microsystems is now well known for allowing superior performances in terms of controlling droplets size distribution. The main advantage of these systems is the possibility of achieving particularly low polydispersity (Bremond and Bibette, 2012; Zhao and Middelberg, 2011). Cross flowing (Y or T junctions)(Tice et al., 2004; Link et al., 2004; Thorsen et al., 2001), flow focusing (Garstecki et al., 2004; Costa et al., 2017) and co-flowing (Nisisako et al., 2006; Perro et al., 2011) are three main categories of geometry used to form a regular droplet train. In addition, the microfluidic technology offers chances to observe the emulsification phenomena in shorter timescale coalescence and ripening with the highly developed fast speed visualization technology (Muijlwijk et al., 2017). However, unlike microfluidics is often associated to industry of the future, the possible flow rate that can be treated within these types of microfluidic devices is quite small, which drastically limits their industrial applications.

The microsystem (Belkadi et al., 2015) proposed in the present study uses head-on impinging configuration and is designed to handle much higher flow rates than most of those traditionally used in microfluidic devices. Due to its

cha... is distributed rather narrowly at higher production rate. In particular, the kinetic energy transported into the collision area is much greater than that in the conventional use of microsystems. For this reason, the microsystem tested in this work is closer, in terms of flow conditions, to the two-impinging-streams emulsifier (Tamir and Sobhi, 1985; Tamir, 1994) that was firstly developed employing spray guns to inject two streams of kerosene in water mixture for face-to-face impinging and thus forming final emulsion. The authors who tested this system also compared it with homogenizer and one stream-impinging-wall system to evaluate its performance, addressing that the new two-impinging-streams device could produce droplets having minimal mean surface area diameter with concentrated distribution. Kiljański (2004) carried out experiments in a modified version setup of the Tamir's apparatus, pointing out there is an optimum distance between the outlets at which the best disintegration of drops would be realized. Later, jets from mini or micro channels impinging in confined space were studied by Mahajan and Kirwan (1994) to characterize micro-mixing effect and timescale in the two-impinging scheme. The jet nozzles they used varied from 0.5mm to 2mm in diameter. These micro-impinging setups known as micromixers (Ait Mouheb et al., 2010) are mainly dedicated for handling miscible fluids; they reveal significant advantages in terms of efficient mixing. It naturally leads to the thoughts of extending their application to the field of immiscible fluids mixing and dispersing, so as to form emulsions. Siddiqui and Norton (2012) and Siddiqui (2014) performed investigations on confined impinging jets mixer for oil-in-water emulsification. Due to the high flow rate tested, the emulsion was generated with turbulent flow conditions, where Reynolds number reached as high as 13000. Droplet mean diameter and size distribution were found to be dependent on jet Reynolds number or energy dissipation rate a lot. Besides, inherent properties of continuous phase and dispersed phase, like viscosity and interfacial tension, showed important effect on the final quality of the emulsion. Tsaoulidis and Angeli (2017) experimentally examined water-oil dispersion in a similar opposed-jets collision configuration at varied hydrodynamic and geometric parameters. It was found that the sum of two jets velocity is the main factor influencing drop size and interfacial area. To conclude on this topic, literature points out that most effort was made on characterizing the droplet size controlled by various parameters, but few studies have been carried out on revealing flow patterns near the impinging region, which is believed to correlate with the mechanism of droplet formation at different flow conditions. This is the primary goal for this work to reach.

Flow patterns of water-oil flows have been described by several authors in mini or micro channels (Wegmann et al., 2006; Bultongez et al., 2017; Saim et al., 2008), however, it is assumed that the flow characteristics concerning oil-water interaction and development inside the microsystem studied in this work will be very distinct from those mentioned above due to impinging flow and relatively higher flowrate conditions used. Meanwhile, the collision space is quite compact. Energy induced to the biphasic flow can be hundred times of that occurring in conventional microfluidic devices. As the transition from inertial flow to turbulent one is expected to occur in the range of Reynolds numbers covered, drastic droplets deformations as well as different mechanisms of droplet breakup are expected. At this stage, to our knowledge, no detailed study on the typology of the flow leaving an impact zone confined into a microchannel has been carried out. Belkadi et al. (2015) have revealed the main features of flow patterns at the scale of the cross; but their work has not checked it at the scale of droplets environment.

To sum up, this work is aimed to characterize the flow pattern in cross-slot microsystems employing head-on impingement of oil and water jets for emulsifying. The flow rate imposed is at mL/min level, which is, according to the literature, two or three orders of magnitude higher than most of those implemented in microfluidics. Besides, two configurations are compared. One is designed as off-axis for the inlet channels of the respective continuous and dispersed phases in order to generate swirl motion of flow in the impingement region for enhancing mixing intensity, which is expected to get emulsion with finer dimension. The other one consists in simple traditional cross-slot geometry, i.e., inlet channels have equal dimensions, which means that swirl flow structure does not occur in it. As a complementary part of this work, droplet size measurement is also carried out at different flow conditions so as to analyze benefits or detriments of the presence of a swirl flow.

2. Theoretical Background

In this section, stress involved in the breakup process of dispersions, that is, emulsion formation is briefly stated

in b
rates.

2.1 Emulsification in viscous flow

Mechanism of emulsion formation in the laminar flow has been disclosed for several decades (Taylor, 1932). The shear stress exerted on a drop in a viscous shear flow is given by:

$$\tau_s = \mu_c G \quad (1)$$

Where μ_c is the viscosity of the continuous phase and G is the velocity gradient on the surface boundary.

The equilibrium pressure difference developed across the interface between two static fluids is known as Laplace pressure:

$$p_L = \frac{2\sigma}{R} \quad (2)$$

Where σ is the interfacial tension and R is radius of the droplet.

Extra energy has to be applied to overcome this pressure in order to deform and break the droplet. As can be observed in eq.(2), the amount of energy to exert on the droplet in order to break it is inversely proportional to its the radius.

Whether the dispersion can split into smaller drops depends on the competition between external force and cohesive force. Based on this, a dimensionless criterion, Weber number, is raised to determine the largest droplet in the diameter of D sustaining in the laminar flow during emulsification:

$$We = \frac{\mu_c G D}{4\sigma} \quad (3)$$

It was reviewed by Walstra (1993) that the critical Weber number for disruption of droplets in simple shear flow is highly determined on the viscosity ratio of two phases in a non-linear pattern.

2.2 Emulsification in turbulent flow

In turbulent flow, the main disruptive stress becomes the dynamic pressure fluctuation inside the flow field resulting from the unstable velocity, which can be represented as:

$$\tau_p \propto \frac{1}{2} \rho_c \overline{u_\lambda^2} \quad (4)$$

u_λ is the velocity difference over the length scale λ . It has to be stressed that turbulent structures larger than the fluid particles are commonly assumed to cause displacement. So, only turbulent structures of a size equal to or less than the fluid particles cause breakup (Andersson and Andersson, 2006). According to the theory of Kolmogorov and Hinze (Kolmogorov, 1949; Hinze, 1955; Davies, 1985), energy cascade contributes most to the understanding of the breakup of dispersions into emulsion. Energy contained in the large structures will not be dissipated to the smaller-scale structures only with transportation, until the Kolmogorov length scale λ_k is reached, which is defined as:

$$\lambda_k = \left(\frac{\nu_c^3}{\varepsilon} \right)^{1/4} \quad (5)$$

Where, ν_c is the kinematic viscosity of the continuous phase, ε is the energy dissipation rate.

In this context, u_λ is related to the local energy dissipation rate and size of the eddies, λ , which is given by:

$$\overline{u_\lambda^2} = C_1 (\varepsilon \lambda)^{2/3} \quad (6)$$

In a stable emulsion system, the equilibrium is established between the turbulent pressure fluctuations tending to deform the drop and the surface tension counteracting the deformation. Again, the ratio between the two stresses can be denoted as Weber number:

$$We = \frac{\rho_c \overline{u_\lambda^2} / 2}{2\sigma / R} \quad (7)$$

Thus the largest droplet in the diameter of D_{max} can be predicted as (replacing eddy size λ to D_{max} as the length scale):

$$D_{max} = C_2 \varepsilon^{-2/3} \left(\frac{\mu_c}{\rho_c}\right)^{1/3} \quad (8)$$

Sprow (1967), Lemenand et al. (2003) and Boxall et al. (2009) show that the average droplet size is proportional to the maximum size:

$$\bar{D} = C_3 D_{max} \quad (9)$$

Developed from the Kolmogorov and Hinze model, a number of studies succeed in scaling droplet size with turbulent flow conditions. Berkaman and Calabrese (1988) proposed a correlation for the Sauter mean diameter D_{32} , as well as for the size distribution function in a static mixer at turbulent flow conditions. What's more, it was found that there are two sub regimes for oil-water emulsifying in high turbulence: inertial sub-range and viscous sub-range. In the inertial sub-range, the maximum drop size is larger than the Kolmogorov length and it is not influenced by the viscosity. However, in the viscous regime, it is reversed (Shinnar, 1961). The fact that the droplet size is smaller than the turbulent eddy size means it requires much more energy dissipation rate to achieve the regime. The maximum size in viscous sub-range can be estimated by:

$$D_{max} = C_4 \sigma \left(\frac{\mu_c}{\varepsilon \rho_c}\right)^{1/2} \quad (10)$$

Vankova et al. (2012) performed systematic experimental study of oil-water emulsification in a "narrow-gap homogenizer" to quantify the effects of a set of parameters (viscosities of the continuous and dispersed phases, oil volume fraction, the interfacial tension and energy dissipation rate) on droplet size as well as distribution in both inertial and viscous sub-ranges. Differences in terms of level of dependency on various investigated factors were enlightened.

3. Experimental setup

The experimental setup to investigate oil-in-water (o/w) emulsification within the impinging microfluidic facility is diagramed in the Fig.1. Continuous phase (water) and dispersed phase (sunflower oil) are supplied into the device by two Armen pumps (AP TRIX 500). Their working pressure can reach up to 200 bar, making fluids flow at higher flowrate (up to 500 mL/min) possible, especially for the more viscous phase. Two weighing scales (Sartorius-MSE 2203) with an accuracy of 0.001 g are used to measure flowrates of water (\dot{m}_c) and oil (\dot{m}_d) by connecting to a NI DAQ module (USB-6009 analog to digital). The sampling rate for the mass flow rate acquisition is 1 Hz. Before flowing into the microchannel, static pressure is monitored at the inlet of water (P_c) and oil (P_d) channels with Gems 31IS series pressure transducers. The measuring range of the pressure sensor is 0-250 bar with the accuracy of 0.25% in the full span. The pressure signal is also recorded via the same DAQ system at the sampling frequency of 100 Hz to ensure the synchronization with mass flow measurement. All connection pipes between the pumps and microchannel are Fluoro-polymer tubing with the internal diameter of 1.55 mm. The emulsion issues from outlets at atmospheric pressure condition and then is collected in a container to perform sampling microscope analysis.

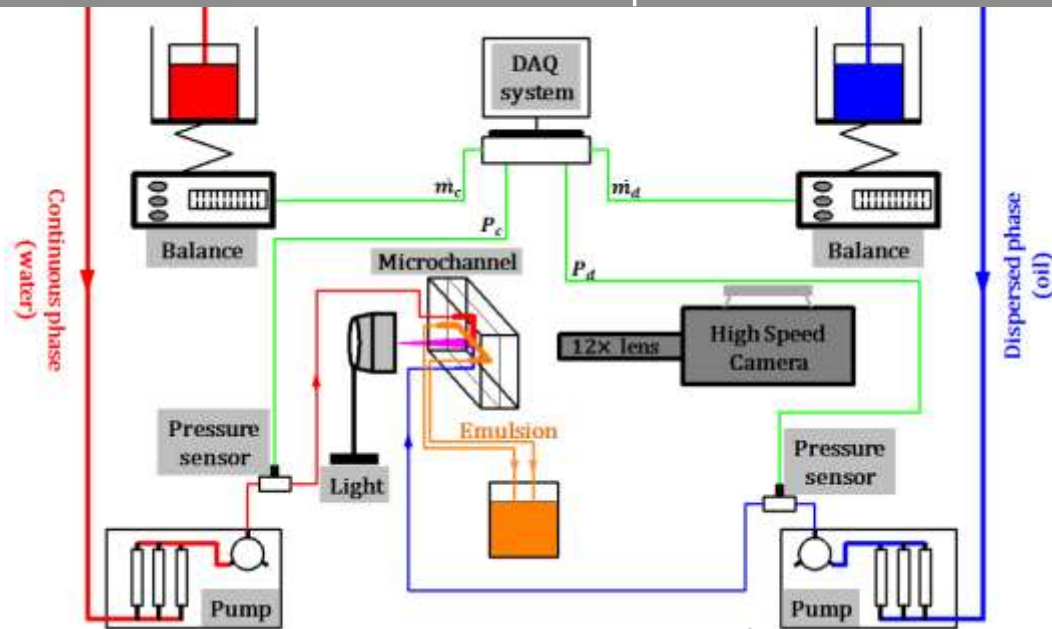


Fig. 1. Experimental setup for oil-in-water emulsification.

3.1 Microfluidic device

The microfluidic devices designed for highly efficient oil-in-water emulsification utilizing impingement configuration of two streams are shown in Fig.2; they have been investigated previously by Belkadi et al. (2016; 2018). Fig.2(a) depicts the 3D layout of the device. Basically, the whole facility is mainly made of two transparent PMMA slabs considering accessibility for optical measurements. One slab is mechanically grooved with square micro channels for the aqueous phase, oil phase and emulsions. The microchannels are arranged in a crossroad format. The other slab covers over it with several bolts and nuts tightened. A rubber gasket is inserted between them to avoid leakage.

The details of the microchannels layout and dimensions are shown in Fig.2(b) and (c). Water channel and oil channel are in the positive and negative X directions respectively with the total length of 20 mm. Water and oil streams develop in the feeding channels and form a head-on impingement to strengthen the interactions and breakup. Generated emulsion flows towards along the two opposite Y directions. The emulsion outlet channels also have a length of 20 mm. Effectiveness of two systems is compared in the present study. Their difference lies in the section area of the oil inlet channel. For both systems, water channel and emulsion outlet channels keep the same square cross section dimensions, which is $600\ \mu\text{m} \times 600\ \mu\text{m}$. As for the oil channel, in one system it is designed to be as same as the water channel in dimensions ($600\ \mu\text{m} \times 600\ \mu\text{m}$); this system is designated as '600-600'. Thus, 600-600 system is characterized by a fully symmetrical geometry. The other one has a smaller size of oil channel, which is $300\ \mu\text{m} \times 300\ \mu\text{m}$. Therefore, it is designated as '600-300' system. It is characterized by an offset of water and oil feeding channels axis in the depth direction (Z) with the magnitude of $150\ \mu\text{m}$. It has to be emphasized that there is no off-axis in Y direction for 600-300 system making two emulsion outlets still symmetrical.

Fig.2(d) and (e) present XZ section plane of the two systems with imposed velocity profiles. The important feature of 600-300 system is that swirl flow structure can be generated in the impingement zone, which may favor emulsification in terms of efficiency and quality. One goal of this work is to investigate the effect of this swirl effect by comparing flow patterns and droplet size with the symmetrical and also more conventional 600-600 system.

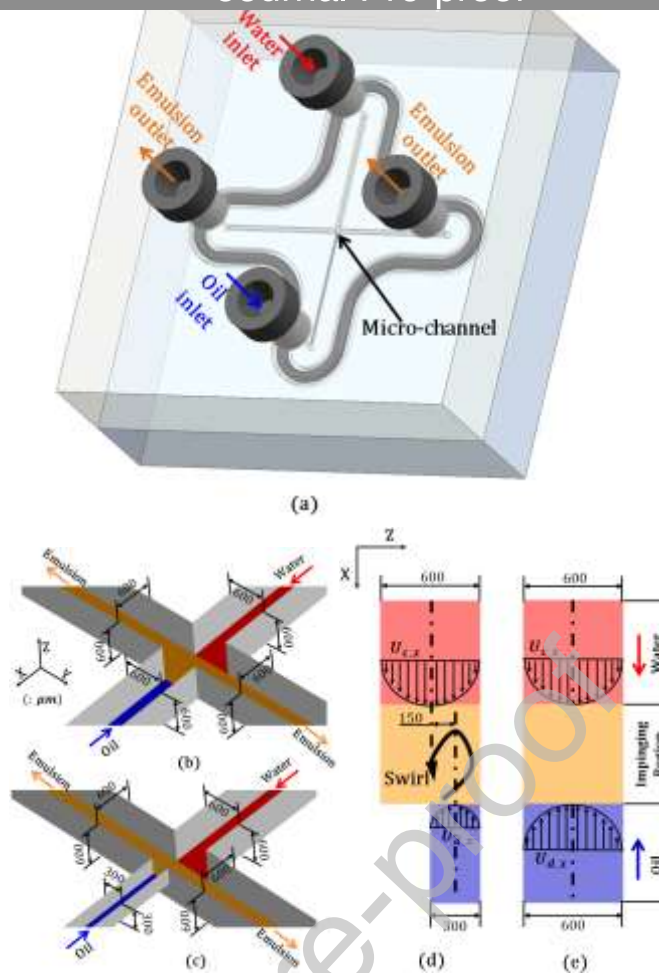


Fig. 2. Microchannel System: (a) microfluidic emulsification device; (b) 600-600 system; (c) 600-300 system; (d) XZ plane of 600-300 system; (e) XZ plane of 600-600 system.

It is important to note a difference between the swirl motion in the present off-axis cross-shaped channels and in other configurations presented by previous studies, such as rotating pipe (Dennis et al., 2014; Lemenand et al., 2014) and stirred system with rotating impeller (Solsvik and Jakobsen, 2015). In the 600-300 system, spiral vortex is generated by the combined effect of tilted impinging plane and confined chamber wall in the cross-shaped channel, rather than caused by the effect of external rotating force or rotated geometry.

3.2 Flow visualization

The flow visualization in the region of interest is carried out by a Photron fast speed camera (FASTCAME SA-X2 1080K M4), whose maximum frame rate is 1080 kHz. The region of interest is only focused on one outlet channel based on the fact that the two outlet channels are in symmetric layout. The flow patterns developed in the two outlet channels are estimated to be similar as preliminary tests were done before optical experiments to evaluate the mass flowrate of emulsion coming from the both outlet channels, and they are found to be the nearly same. What's more, a previous study (Belkadi et al., 2015) has roughly checked the main features of flow patterns in both outlet channels at the same time using a high speed camera. However, the observations achieved in this preliminary study concerned a too large region of interest to get a precise idea on break-up phenomena at the scale of droplets environment. So, only one outlet channel is observed in the current study to save pixels for showing more details. To balance the spatial and temporal resolutions, the shooting frame rate in the present study on flow patterns is selected to be 300 kHz, hence the exposure time is limited to be the longest available ($1/583784$ in seconds) for this frequency. A Lavision high magnification ($12\times$) zoom lens is used to allow observations at the micrometer scale in the emulsification facility. The focus of the lens is adjusted in the channel depth. Considering the region of interest in the observation, the spatial resolution is $2.4 \mu\text{m}/\text{pixel}$. Because of high speed capturing images with such a large zoom lens at so short exposure time, an external powerfull light source is necessary to illuminate the microchannel

lamp is located at the opposite side and facing the camera beyond the transparent microchannel so as to enhance the brightness in a great extent. Attention is paid on the fact that the use of the lamp does not warm up the fluid flowing through the studied microsystem.

3.3 Droplet size measurement and characterization of the size distribution

The size of oil droplets is measured in the o/w emulsion sample collected from the container, this one receiving emulsion from both outlet microchannels (shown in Fig.1). As mentioned above, there should not be a significant difference between the emulsions from the two outlets in terms of droplet statistical results since the flow patterns are similar. Moreover, the collected testing sample from the container can be viewed as a comprehensive result of the final emulsion from the two outlet channels. An Olympus upright optical microscope is adopted with assembling 20 \times and 50 \times objective lens chosen case by case. The high resolution image shoot by the microscope is then analyzed manually. The characteristic dimension of dispersed drops is obtained from a sample of a sufficient number of droplets. The number of measured droplets is determined based on the convergence of the mean diameter to a stable value.

In order to conduct quantitative comparison, statistical analysis of droplet diameter in the testing sample is performed on the microscope images. Emulsification quality is evaluated by several parameters defined as follows.

The arithmetic mean diameter of the droplets D_{10} :

$$D_{10} = \frac{1}{n} \sum_{i=1}^n D_i \quad (11)$$

Where, n is the number of the analyzed droplets, D_i denotes diameter of each droplet.

Based on the arithmetic mean diameter, the standard deviation is calculated as:

$$\delta = \sqrt{\frac{\sum_{i=1}^n (D_i - D_{10})^2}{n}} \quad (12)$$

The Sauter mean diameter (SMD) D_{32} is defined as the diameter of a sphere that has the same volume/surface area ratio as a collection of droplets. It is important since the active surface between oil-water two phases in the emulsion implies the potential interfacial energy stored. The calculation is given as:

$$D_{32} = \frac{\sum_{i=1}^n D_i^3}{\sum_{i=1}^n D_i^2} \quad (13)$$

Another essential parameter is the polydispersity index (PdI), which is the indicator of the size distribution uniformity. A low value of PdI indicates that droplets are rather monodispersed. The ideal monodispersed emulsion has PdI value equaling to zero. This parameter is defined as the square of the standard deviation-to-arithmetic mean diameter ratio:

$$PdI = \left(\frac{\delta}{D_{10}} \right)^2 \quad (14)$$

Fig.3 shows the convergence curve in 600-600 system for one flow rate example case. It is confirmed that after around 500 droplets measured, the droplet arithmetic mean diameter, the Sauter mean diameter and standard deviation all approach to the final stable results. So, 500 droplets will be further analyzed.

It may be emphasized that using an optical microscope leads to a physical cut-off of the size distribution for droplets diameter under about 1 μm . However, it also may be stressed that using a laser sizer leads to some bias when droplets are aggregated. Therefore, in our opinion, there is no ideal method. In this kind of work, the characterization of droplets size distribution is mostly interesting for the establishment of comparisons between emulsions obtained at various conditions.

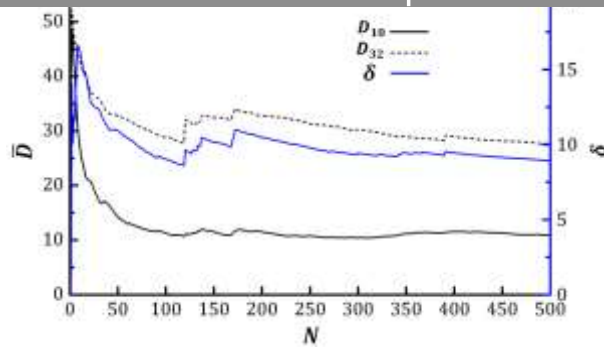


Fig. 3. Convergence of mean droplet diameter and standard deviation.

3.4 Test conditions

As mentioned above, the continuous and dispersed phases used for o/w emulsification are water and oil, respectively. Their main characteristics at 25°C are recapped in Table 1. The surface tension and interfacial tension have been measured using a Kruss K-12 tensiometer. The viscosity of the fluids has been obtained using a Thermo Scientific Haake Mars III rheometer. The uncertainty of the tension and viscosity measurements are estimated to be 5% and 1%.

Table 1. Characteristics of the used fluids (at 25°C).

Liquids at 25°C	Tap water	Sunflower oil
ρ (kg/m ³)	998	865
μ (mPa s)	0.91	52.2
γ (mN/m)	73.5	33.7
σ (mN/m)	27.6	
Supplier	Nantes métropole	Carrefour

During the experimental procedure, preset values of water and oil flow rate are input into the pump control systems based on targeted Reynolds number and oil volume fraction in the emulsion. Reynolds number based on the aqueous phase is designed to be varied from 1000 to 7000 and oil over water volume fraction is ranging from 3% to 30% with the interval of 3%. Specifically, the water flowrate set values are 50, 75, 100, 125, 150, 175, 200, 225, 250 in mL/min. The resulting oil phase flowrate changes from 2 mL/min to 70 mL/min roughly according to the different cases.

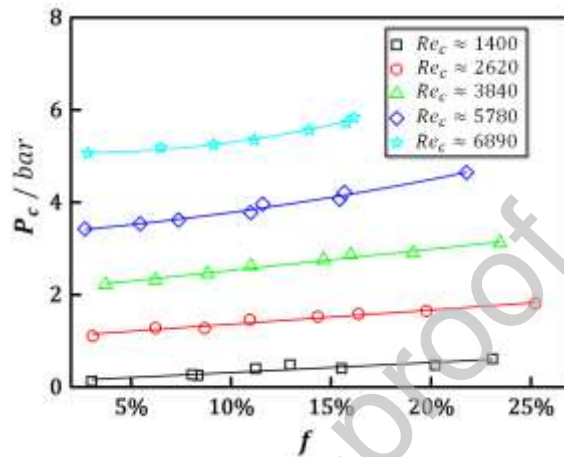
4. Results and discussion

4.1 Pressure at the channel inlets

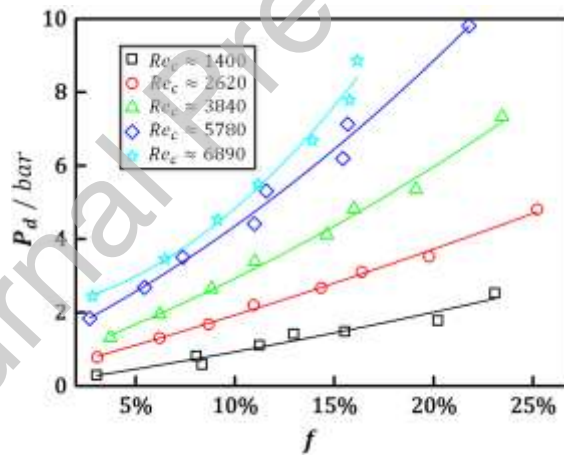
As shown in Fig.4, the inlet pressure of water and oil channels in 600-600 system are monitored to weigh the effort made by the pumps to reach certain conditions of Reynolds number, Re_c , and dispersed phase volume fraction, f . It's reasonable that the inlet pressure increases with Reynolds number as well as oil fraction for both channels because flow rate of water or oil grows. Also, the inlet pressure of the water channel is more sensitive to the variation of Reynolds number compared to oil fraction. To be specific, at the same Re_c case, the pressure rises gently as the volume fraction of oil phase increases. While it is of significant difference that pressure at the inlet oil channel gets drastic augmentation when the volume ratio of oil phase gets higher. It is caused by the high viscosity of the oil phase inducing considerable friction between the flow and channel walls even with low superficial velocity. As the dispersed phase volume takes up over 15% in the o/w emulsion, the inlet pressure of oil channel exceeds that for water channel, but they are still in a comparable level. Going up with Reynolds number, the trend is in the linear pattern at lower Re_c condition, but it goes to be the second power law when Re_c reaches its highest value ($Re_c = 6890$).

As for 600-300 system, the results are presented in Fig.5. Quite the same trend is observed than with 600-600

system. For example, at the highest Re_c condition, the pressure at the oil channel inlet is about 1.5 times of that for the water channel in 600-600 system, but this value goes as high as 6.7 in 600-300 system. Overall, the inlet pressure is higher in 600-300 system if compared to 600-600 system, at given flow rates, especially for the oil channel. It is because that the cross section of oil channel for 600-300 system is only quarter of that for 600-600 system. At the same flowrate condition, the velocity of oil flow in 600-300 system is almost four times of that in 600-600 system. Higher velocity induces greater friction between the flow and the channel and then pressure drop is enhanced, which means that more pumping power is required in oil channel of 600-300 system. Higher oil flow velocity also leads to a higher resistance to the opposite flow (from water channel), so the inlet pressure of water channel in 600-300 system will also be a little higher than that in 600-600 system.

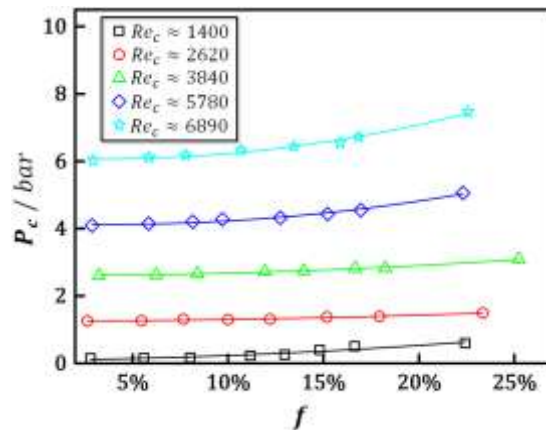


(a) Water channel

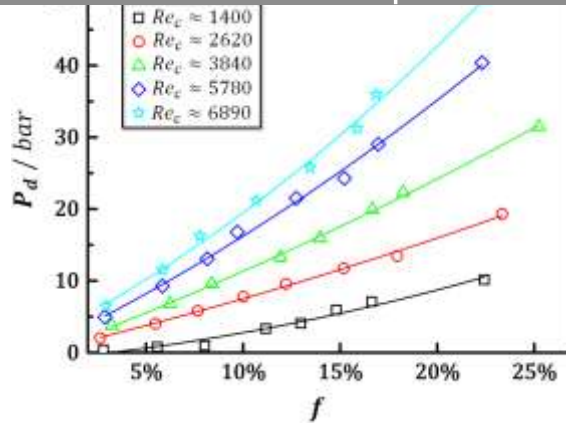


(b) Oil channel

Fig. 4. Channel inlet pressure for 600-600 system.



(a) Water channel



(b) Oil channel

Fig. 5. Channel inlet pressure for 600-300 system.

4.2 Flow patterns

Flow characteristics at the two-phase stream impinging region and near field downstream are captured by the high speed camera to visualize emulsification process and reveal the droplets formation mechanism at different flow conditions. It is observed that the interacting oil-water flow can be mainly partitioned into three typical regimes that are presently designated as: “stratified flow”, “thin filament” and “drops cloud”. As shown in Fig.6, the observation of the interface of the phases recorded at small, moderate and high Re_c conditions shows that similar flow patterns emerge from both impinging configurations (600-600 system and 600-300 system) in the same flow regime, which will be elaborated in the following section in detail.

- **Regime I: “Stratified Flow”.** The flow rate of the continuous phase is small, so hence the Reynolds number. Oil stream presents to be thickly wavelike after colliding with the water flow. No distinguished breakup of the dispersion but only stratified flow is identified in this impingement region. Because of the density difference and inherent perturbation inside of this type of head-on collision, Rayleigh instability causes the oil-water interface to be corrugated (Sharp, 1983). Developing in emulsion channels towards the outlets, small amount of droplets in extremely large size can probably be shed off from the interface.
- **Regime II: “Thin Filament”.** In this stage, superficial velocity of the water phase increases in some extent leading to viscous shear stress between two phase flows undergoing a considerable increase. It promotes the breakage of the oil stream, thus longer and thinner filaments with small droplets around them can be seen. In addition, due to the higher energy induced by impingement, the droplets are not monodispersed and generated in an orderly sequential way. Basically, the breakup mechanism is similar in the regime I and II ; it results from the competition between the disruptive viscous stress and cohesive interfacial stress.
- **Regime III: “Drops Cloud”.** With the rise of both continuous and dispersed phase flow rates, greater amount of kinetic energy is input into the impingement area causing turbulent mixing of two streams. Strong unsteady turbulent flow splits the stream or large droplet, forming a cloud of small drops rapidly. The principle behind that is the dynamic pressure fluctuation which exerts as external destructive stress; oil phase is teared apart into small particles at turbulent flow conditions. Once Laplace stress on the two-phase interface is not great enough to counteract that, the droplets will breakup very easily and promptly. In addition, droplet size mainly depends on the energy dissipation rate, so it is comparable with the Kolmogorov length λ_k .

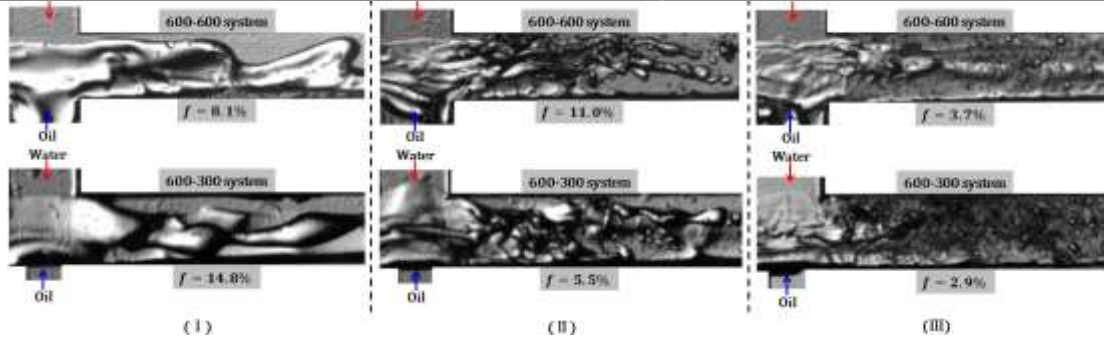


Fig. 6. Flow patterns (Regime I, $Re_c \approx 1400$; Regime II, $Re_c \approx 2620$; Regime III, $Re_c \approx 5780$).

Although the flow pattern is primarily related to Reynolds number, oil volume fraction in the emulsion has also some effect. Fig.7 depicts the flow characteristics at the medium Reynolds number conditions by varying the dispersion fraction for both microsystems. It clearly shows that in the thin filament region, if more oil is pumped to collide with the constant amount of water, the oil stream acts to be more and more difficult to breakup into fragments. For 600-600 system, this phenomenon can be seen at the highest investigated oil fraction case ($f = 25.2\%$). However, the same scenario is observed with slight lower f value ($f = 17.9\%$) in 600-300 system.

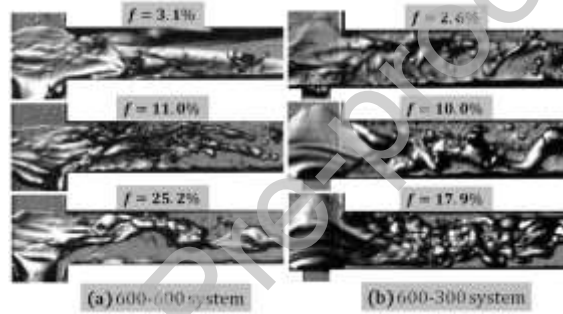


Fig. 7. Effect of oil volume fraction on flow patterns ($Re_c \approx 2620$).

A simplified analysis is performed in the impingement area so as to get insight of reasons causing the behavior stated above. As diagramed in Fig.8(a) with the coordinate, water and oil flows impact with each other through YZ plane in the opposite directions, and emulsion outflows are pointing to positive and negative Y axis correspondingly. Looking from the XY plane, viscous stress are generated in two areas, which are labeled with A and B in Fig.8(b). Region B is where two streams undergo a direct contact and region A is where they merge. In region A, because of two phases are immiscible, continuous phase and dispersed phases develop to the downstream with the superficial velocity of $U_{c,y}$ and $U_{d,y}$. Dependent on the flow rates, the velocity gradient ($U_{c,y} - U_{d,y}$) between them leads to great stress formed in the shear layer. In all cases for 600-600 system and most cases for 600-300 system of investigated flow conditions, $U_{c,y}$ is higher than $U_{d,y}$. When the Reynolds number is kept constant, raising the phase fraction implies an increase of $U_{d,y}$, which results in the decrease of the velocity gradient. Therefore, lowering the viscous stress makes it difficult to overcome the interfacial stress and then to breakup oil droplets. This is the reason why the emulsification doesn't perform efficiently at higher content of oil phase in the thin filament regime for both emulsifiers, i.e. 600-600 system and 600-300 system.

Recognizing this, it is then quite straightforward to understand the differentiation of the two systems in terms of oil volume fraction effect. Oil channel section in 600-300 system configuration is only quarter of that for 600-600 system. At a given flow conditions, velocity of oil flow is absolutely greater in 600-300 system than in the other microsystem. Once oil fraction is high enough, it even exceeds the water flow velocity. In contrast, this emulsifier with unequal size for two phase channels produces relatively smaller disruptive stress for breakage in region A. It explains why the flow mode switch occurs at slightly lower oil volume fraction for 600-300 system compared with 600-600 system.

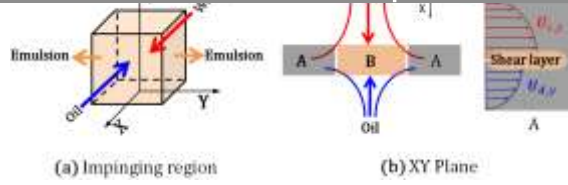
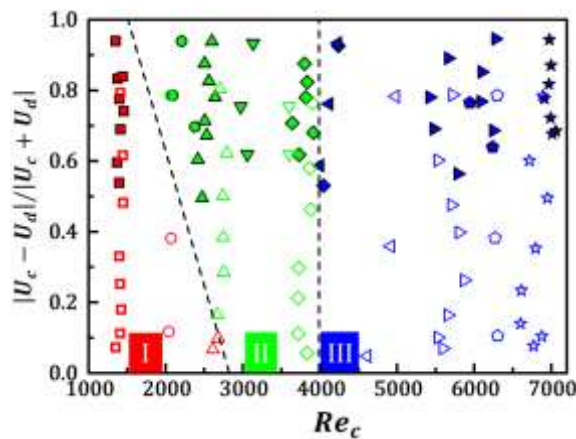


Fig. 8. Diagram of viscous stress generation in the collision area.

On the other hand, benefits of the 3D-swirl flow structure shouldn't be ignored, which is believed to play a significant role in Region B indicated in Fig.8(b). The following discussion is referred to the XZ plane (referred to Fig.2(d) and (e)). Water and oil jets with assumed velocity profiles ($U_{c,x}$ and $U_{d,x}$) meet together and then interact in the impingement zone. Due to off-axis layout of water and oil microchannels, a great velocity gradient is generated there. Moreover, a stagnation point ($U_x = 0$) stands in the line connecting velocity cores of the two streams since U_x goes through one direction to the other. This stagnation point is the center of the recirculation flow. Angular momentum imposed on fluid causes its rotation and deformation in the collision area. The swirl strength can be simply represented by the sum of continuous and dispersed phases velocity magnitude, $U_{c,x} + U_{d,x}$. However, this swirl effect is absent in 600-600 system, which means that breakup of the dispersed phase jet in zone B of 600-300 system is significantly different than in 600-600 system.

Based on above discussions, the charts indicating flow regime for both systems are mapped in Fig.9(a) and Fig.9(b). The oil volume fraction effect is interpreted as absolute normalized superficial velocity difference ($|U_c - U_d|/|U_c + U_d|$) or absolute normalized momentum flux difference ($|I_c - I_d|/|I_c + I_d|$) between two phases separately. Momentum flux, I , is defined as ρU^2 . Although the gap of the oil-water velocity difference for two systems is smaller compared with momentum flux difference, the general trend on different flow pattern regions doesn't alter because of velocity highly correlated with the momentum.

Regardless of geometry, the decisive parameter responsible for the flow patterns of oil-in-water emulsification in the present studied microchannels is Reynolds number. The interacting oil-water flow pattern changes from the viscosity dominated region to the turbulence dominated region at the critical Re_c around 4000. In the viscosity dominated region (I & II), velocity variance factor weighs a lot. Flow patterns in stratified flow region certainly present to be in intensified instability style when Re_c is less than 1500. The prominent feature shows up in the region of Reynolds number ranging from 1500 to 4000, where the flow pattern is supposed to be in the thin filament region. The small velocity difference between two phase flows could pull it back into the stratified flow regime, which has been clarified above. With regard to the distinction for the two microfluidic device configurations, it indicates that at the same Reynolds conditions, flow pattern in 600-300 system tends to more likely lies into the stratified flow regime with high content of oil in the emulsion due to the much lower velocity difference existed there. Another clue obtained from the flow regime map is that the swirl flow in the interaction region for 600-300 microchannel may not help too much in terms of dispersed phase breakup, especially in the thin filament regime with higher volume ratio of oil. This will be proved in the following sections.



(a) $|U_c - U_d|/|U_c + U_d|$ vs. Re_c

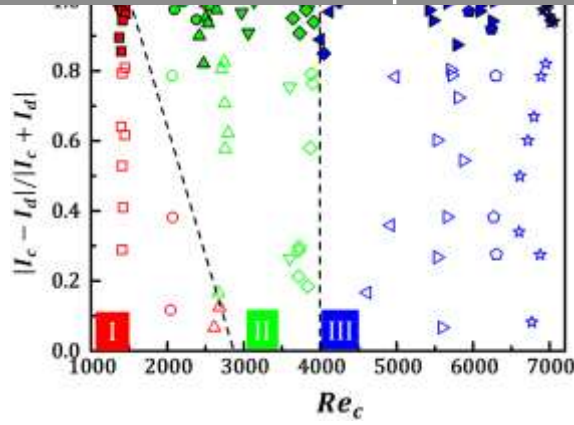
(b) $|I_c - I_d|/|I_c + I_d|$ vs. Re_c

Fig. 9. Flow regime map ([shape of symbol] ‘square’: $Re_c \approx 1400$; ‘circle’: $Re_c \approx 2140$; ‘upward-pointing triangle’: $Re_c \approx 2620$; ‘downward-pointing triangle’: $Re_c \approx 3540$; ‘diamond’: $Re_c \approx 3840$; ‘left-pointing triangle’: $Re_c \approx 4480$; ‘right-pointing triangle’: $Re_c \approx 5780$; ‘pentagon’: $Re_c \approx 6590$; ‘star’: $Re_c \approx 6890$. [fill of symbol] solid: 600-600 system; hollow: 600-300 system. [color of symbol] red: “Stratified Flow” regime; green: “Thin Filament” Regime; blue: “Drops Cloud” Regime).

4.3 Droplet size and size distribution

To verify the assumption on swirl effect in 600-300 system proposed at the end of the previous section, experimental measurements of emulsion droplets size and size distribution are carried out using a microscope. Two flow conditions corresponding to thin filament and drops cloud regions are tested respectively. For the case in the thin filament regime, the water volume flowrate is maintained at 95.2 ± 4.3 mL/min while the oil flowrate is kept at 12.8 ± 0.4 mL/min ($Re_c = 2640$, $f = 11.9\%$). For the condition in the drops cloud regime, the water flow rate is controlled at 244.3 ± 7.0 mL/min and the oil flow rate is 31.6 ± 0.3 mL/min ($Re_c = 6770$, $f = 11.5\%$). Tween20 (1 wt.%) as surfactant is added to stabilize the emulsion testing sample for a few minutes before finishing the microscope observation.

Fig.10 and 11 are the testing sample images of oil-in-water emulsification droplets taken by the microscope at both cases. $20\times$ and $50\times$ magnification objectives are used respectively for the low and high flowrate conditions. It points out that the oil droplets are dispersed rather sparsely in the thin filament regime. Also, the variance in size for the large and small droplets is clearly identified showing that the emulsion is a typical polydispersed system (Fig.10) and indicating that various mechanisms of break-up may occur in microsystems. In addition, the range of size seems more pronounced in 600-300 system. However, it is a totally different scenario when Reynolds number is raised. As depicted in Fig.11, oil droplets are compactly dispersed in the emulsion with less variation in terms of size at $Re_c \approx 6770$. Knowing that the smaller the size distribution, the more stable the emulsion, 600-300 system seems to be more efficient as it tends to produce droplet more uniformly.

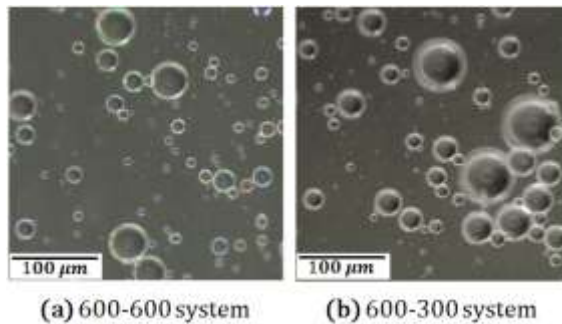


Fig. 10. Microscope images of o/w emulsification in the transitional flow region ($Re_c \approx 2640$, $f = 11.9\%$).

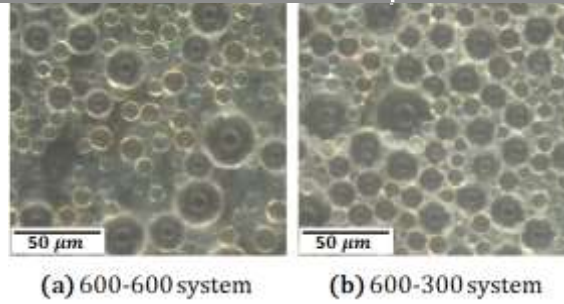
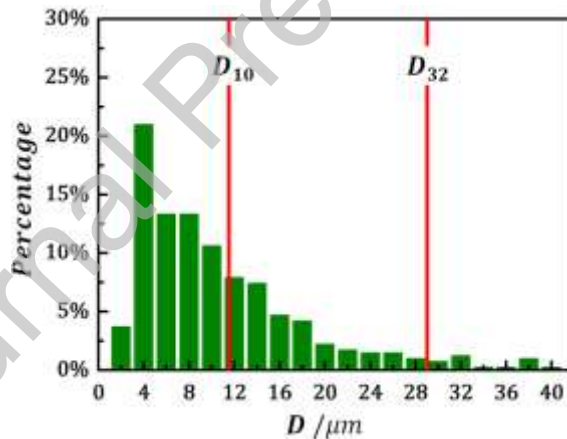
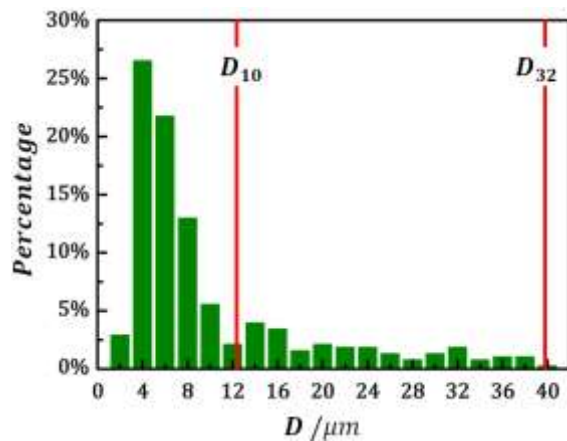


Fig. 11. Microscope images of o/w emulsification in the turbulent flow region ($Re_c \approx 6770$, $f = 11.5\%$).

As shown in Fig.12, droplet size distribution for the o/w emulsification with head-on impinging in the thin filament regime is presented. The overall trend tells that the drops are dispersed in a manner of log normal distribution. It can be found that the number percentage of drops in diameter less than $6 \mu\text{m}$ is 38.0% and 51.2% respectively for 600-600 system and 600-300 system, which implies that more fine drops are formed in 600-300 system. Meanwhile, the number percentage of drops in diameter higher than $22 \mu\text{m}$ is 9.3% and 12.2% respectively for 600-600 system and 600-300 system. That is, 600-300 microchannel can produce more oil drops with relatively large diameter than 600-600 system. In the range of size $[10 \mu\text{m} - 40 \mu\text{m}]$, distribution is much more uniform for 600-300 system than 600-600 system configuration. That is the reason why D_{10} in the two systems are close, but the Sauter mean diameter D_{32} is much greater in 600-300 system. So the swirl flow structure may be beneficial to the formation of very small droplets in the impingement area, whereas it definitely has detrimental effect in the downstream shear induced breakup, then it preserves a lot of very big droplets in the emulsion. This verifies previous observation and assumption made based on flow patterns.



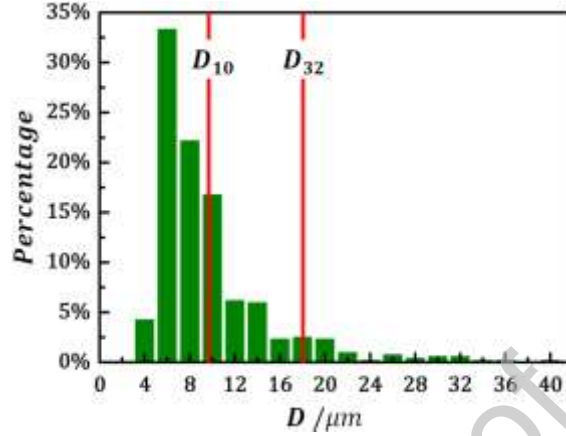
(a) 600-600 system



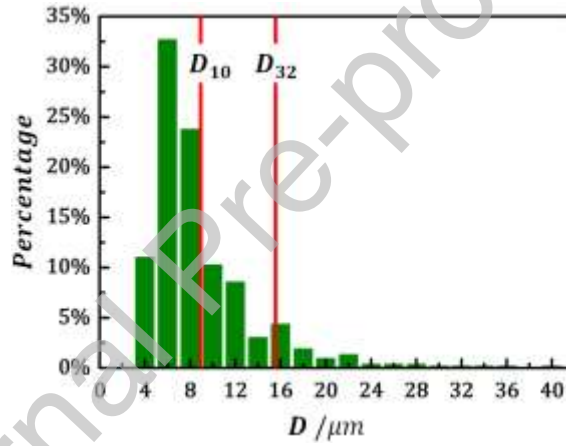
(b) 600-300 system

Fig. 12. Droplet size distributions at low flow condition ($Re_c \approx 2660$).

in no matter 600-600 system (2.9%) or 600-300 system (1.7%). So the mean diameter of drops decreases compared to that in thin filament regime. Fig.13 clearly shows that the disparity of two systems lies in that 600-300 microchannel produces more extreme small droplets. Specifically, the amount of drops with diameter less than 4 μm occupies 11.0% of total droplets, which is only 4.2% for 600-600 system. This is consistent with what happens in thin filament regime and it could be attributed to the positive effect brought by swirl motion.



(a) 600-600 system



(b) 600-300 system

Fig. 13. Droplet size distributions at high flow condition ($Re_c \approx 6770$).

Table.2 summarizes the droplet size and size distribution results. To conclude, maximum drop diameter, droplet mean diameter and polydispersity all decrease when the flow pattern is varied from thin filament regime to the drops cloud. So the great advantage of turbulence induced breakup is to promote smaller droplet with more narrow distribution. At lower Re_c case, arithmetic mean diameter of oil droplets in 600-300 system is slightly higher than that in 600-600 system, but the difference is not as much distinguished as the Sauter mean diameter (D_{32} is 27.6 μm for 600-600 microchannel and 38.6 μm for 600-300 microchannel). More surprisingly, the gap of polydispersity between two systems is extremely large, proving again that the monodispersity of droplets distribution in the 600-300 system is far more than poor with the PdI reaching over 100%. In contrast, at higher Re_c case, 600-300 system performs slightly better than 600-600 system because of oil droplets dispersed in relatively smaller diameter.

Weber number is also calculated to characterize the ratio of inertial force and interfacial force on the droplets:

$$We = \frac{\rho_c U_a^2 D_{10}}{\sigma} \quad (15)$$

It is observed that inertial stresses acting on the drops increase greatly as flow turns more turbulent. Moreover, 600-300 system has potential of releasing more inertial force to disperse oil phase than 600-600 system, especially at high turbulent conditions.

Condition	system	D_{max} (μm)	D_{10} (μm)	D_{32} (μm)	Pdl	We
$Re_c=2640$	600-600	59.1	10.9	27.6	67%	0.10
$f=11.9\%$	600-300	66.5	11.6	38.6	106 %	2.5
$Re_c=6770$	600-600	49.9	9.7	18.1	33%	0.70
$f=11.5\%$	600-300	40.8	8.9	15.7	30 %	10.8

Finally, the energy dissipation rate (ε) of the two microsystems at all tested cases are evaluated. The energy dissipation rate for this head-on collision micro-mixer can be estimated as follows (Johnson and Prud'homme, 2003; Siddiqui et al., 2009):

$$\varepsilon = \left(\frac{\dot{m}_c U_c^2}{2} + \frac{\dot{m}_d U_d^2}{2} - \frac{\dot{m}_e U_e^2}{2} \right) / \rho_e V_{iz} \quad (16)$$

Where \dot{m}_c , \dot{m}_d and \dot{m}_e are the mass flow rates of continuous phase, dispersed phase and outlet emulsion flow. U_c , U_d and U_e are the superficial velocities of continuous phase, dispersed phase and outlet emulsion flow. ρ_e is the density of mixture or emulsion. V_{iz} denotes the volume of mixing zone, which is assumed to be $600 \mu\text{m} \times 600 \mu\text{m} \times 600 \mu\text{m}$ for both systems. The energy dissipation rate represents the net kinetic energy carried by two impinging jets into the mixing zone utilized for emulsion production per mass emulsion and per time. If emulsification happens at turbulent flow conditions, energy dissipation rate is directly related to the dispersed droplet size.

Energy dissipation rate is calculated to vary over a range of 5-1000 W/kg for Reynolds number of 1000-7000 for current microsystems. This is much larger than the mean energy dissipation rate in a stirred tank, which typically lies in the range of 0.1-100 W/kg. When the flow rate approaches turbulent conditions, the energy dissipation rate goes up rapidly leading to breakup much more intensely. Difference of ε is hard to distinguish for two systems at low Reynolds number conditions. Once Re_c is increased up to around 4000, energy dissipation rate in 600-300 system tends to be higher than that in 600-600 system. This explains why 600-300 system performs slightly better than 600-600 system in the drops cloud regime.

In terms of drop size, the correlation between Sauter mean diameter and energy dissipation rate for the currently studied microchannels is compared to data from other studies concerning T-type confined impinging-jets (CIJ) in Fig.14. The CIJ was investigated by Tsaoulidis et al. (2017) to disperse directly Exxsol 80 oil in the water at relatively lower energy dissipation rate conditions, which leads to the drop size to be much greater (generally over $100 \mu\text{m}$). Another reason for generating so large drops in their system is probably that no surfactant is utilized.

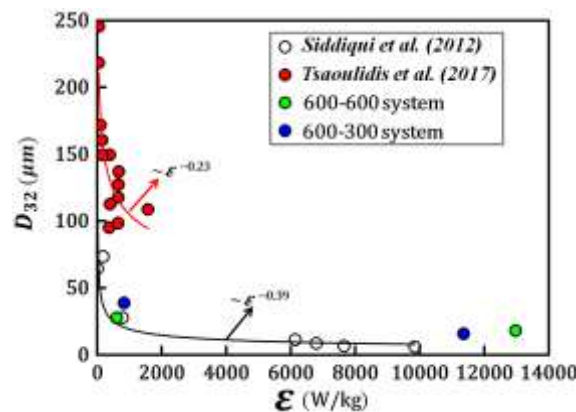


Fig. 14. Sauter mean diameter vs energy dissipation rate for different configurations.

Siddiqui et al. (2012) also investigated a CIJ device to characterize oil-in-water (sunflower oil dispersed in distilled water) emulsification at turbulent conditions. The investigated energy dissipation rate is comparable with

the condition, droplet size fabricated by their CIJ device is close to that in 600-600 system, both being smaller than with 600-300 system. When the energy dissipation rate reaches higher level, our microsystems performance does not seem to be as good as the system designed by Siddiqui et al. (2012). It is attributed to the fact that the two impinging streams in their study are coarse emulsions (pre-emulsion), so their trials do not correspond to a direct emulsification. To sum up, the microsystem proposed in the present study utilizing head-on collision configuration works quite efficiently on the point of view of the mean drop size obtained.

5. Conclusion

Experimental study on oil-in-water emulsification process has been performed to characterize the flow patterns in a large range of Reynolds number [$\sim 1000-7000$] and using ad-hoc designed microfluidic devices utilizing head-on collision configuration. Droplets size distribution has also been characterized at two flow conditions. Flow visualization with high speed camera has been focused in the impact area of the fluids; it reveals the flow regime partition of water-oil two phase flow near the impingement region under the effect of the Reynolds number based on the aqueous phase, Re_c , and oil volume fraction, f . Droplet size and size distribution have been measured at high dispersed phase volume fraction. The results stress the great difference of oil-water flow interaction and development developed in the microchannels studied here at relatively high flow conditions, compared to those occurring in conventional microfluidic devices working at low flow rate. Moreover, the emulsification mechanism in viscous region as well as it occurring in drops cloud regime are discussed for the presently studied microfluidic geometries. The main observations and conclusions brought from this study could be summarized as follows:

- Re_c shows dominant effect on flow patterns in the vicinity of impingement region, which can be mainly divided into three regimes: "Stratified Flow", "Thin Filament" and "Drops Cloud" respectively. Strong instability of stratified flow with seldom droplet formation is the remarkable feature in the stratified flow regime whereas great chaos inducing promptly oil breakup is the typical phenomenon observed in the drops cloud regime.
- At medium Reynolds number conditions, $Re_c \in [\sim 2000-3000]$, a switching from thin filament pattern to stratified flow pattern is observed if high oil volume fraction is involved. As a matter of fact, it implies a decrease of the velocity gradient in the emulsion channel between two phase flows that leads to the flow mode switching. And it has been shown to be more likely to happen in 600-300 system since its design of oil and water feeding channels at unequal size is favorable for narrowing the velocity gap of two phases.
- A transition to "drop clouds" regime is observed at Re_c higher than ~ 4000 . Based on a comparison of droplet size and size distribution results at high oil volume fraction, 600-300 system performs better as smaller mean droplet diameter and more narrow distribution are obtained at high Reynolds number condition. This is attributed to the higher energy dissipation rate involved, compared to 600-600 system.

To conclude, the studied microchannel systems used for emulsification in the present work perform well at turbulent conditions. As a matter of fact, the 600-300 system is designed to be operational in such a way that it can be more widely applied for industrial tasks than conventional microfluidics devices can do. This study proves that this kind of impingement configuration can work efficiently for the sake of industrial emulsion production at high flow rates. Future work should be focused on the drop deformation and breakup details in the device.

Credit Author Statement :

Yongbin Ji: Experiments, Data Analysis and Writing Original Draft,

Jérôme Bellettre: Conceptualisation, Scientific Project Management, Funding Acquisition and Supervision.

Agnès Montillet: Conceptualisation, Data Analysis and Validation.

Patrizio Massoli: Methodology, Funding Acquisition and Supervision.

The authors gratefully acknowledge the support of program funded by Région Pays de la Loire (Chaire "Connect Talent") on Optical Diagnostics for Energy.

References

- Ait Mouheb, N., Montillet, A., Sollicec, C., Havlica, J., Legentilhomme, P., Comiti, J., Tihon, J., 2011. Flow characterization in T-shaped and cross-shaped micromixers. *Microfluid. Nanofluid.* 20, 1185-1197.
- Andersson, R., Andersson, B., 2006. On the breakup of fluid particles in turbulent flows. *AIChE J.* 52, 2020-2030.
- Belkadi, A., Tarlet, D., Montillet, A., Bellettre, J., Massoli, P., 2015. Water-in-oil emulsification in a microfluidic impinging flow at high capillary numbers. *Int. J. Multiphase Flow* 72, 11-23.
- Belkadi, A., Tarlet, D., Montillet, A., Bellettre, J., Massoli, P., 2016. Study of two impinging flow microsystems arranged in series. Application to emulsified biofuel production. *Fuel* 170, 185-196.
- Belkadi, A., Montillet, A., Bellettre, J., 2018. Study of two impinging flow microsystems arranged in series. Application to emulsified biofuel production. *J. Energ. Resour. Technol.* 140, 012202.
- Berkman, P.D., Calabrese, R.V., 1988. Dispersion of viscous liquids by turbulent flow in a static mixer. *AIChE J.* 34, 602-609.
- Boxall, J.A., Koh, C.A., Sloan, E.D., Sum, A.K., Wu, D.T., 2009. Measurement and calibration of droplet size distribution in water-in-oil emulsions by particle video microscope and a focused beam reflectance method. *Ind. Eng. Chem. Res.* 49, 1412-1418.
- Bremond, N., Bibette, J., 2012. Exploring emulsion science with microfluidics. *Soft Matter* 8, 10549-10559.
- Bultongez, K.K., Derby, M.M., 2017. Investigation of oil-water flow regimes and pressure drops in mini-channels. *Int. J. Multiphase Flow* 96, 101-112.
- Chen, H.T., Middleman, S., 1967. Drop size distribution in agitated liquid-liquid systems. *AIChE J.* 13, 989-995.
- Costa, A.L.R., Gomes, A., Cunha, R.L., 2017. Studies of droplets formation regime and actual flow rate of liquid-liquid flows in flow focusing microfluidic devices. *Exp. Therm. Fluid Sci.* 85,167-175.
- Davies, J.T., 1985. Drop sizes of emulsions related to turbulent energy dissipation rates. *Chem. Eng. Sci.* 40, 839-842.
- Dennis, D.J.C., Seraudie, C., Poole, R.J., 2014. Controlling vortex breakdown in swirling pipe flows: experiments and simulations. *Phys. Fluids* 26, 053602.
- Galus, S., Kadzińska, J., 2015. Food applications of emulsion-based edible films and coatings. *Trends Food Sci. Technol.* 45, 273-283.
- Garstecki, P., Gitlin, I., Diluzio, W., Whiteside, G.M., 2004. Formation of monodisperse bubbles in a microfluidic flow-focusing device. *Appl. Phys. Lett.* 85, 2649.
- Habchi, C., Lemenand, T., Valle, D.D., Peerhossani, H., 2009. Liquid/liquid dispersion in a chaotic advection flow. *Int. J. Multiphase Flow* 35, 485-497.
- Hinze, J.O., 1955. Fundamental of hydrodynamic mechanism of splitting in dispersion process. *AIChE J.* 1, 289-295.
- Solsvik, J., Jakobsen, H.A., 2015. Single drop breakup experiments in stirred liquid-liquid tank. *Chem. Eng. Sci.* 131, 219-234.
- Johnson, B.K., Prud'homme, R.K., 2003. Chemical processing and micromixing in confined impinging jets. *AIChE J.* 49, 2264-2282.
- Joscelyne, S.M., Trägårdh, G., 2000. Membrane emulsification-a literature review. *J. Membr. Sci.* 169, 107-117.
- Kiljański, T., 2004. Preparation of emulsions using imping streams. *AIChE J.* 50, 1636-1639.
- Kokal, S.L., 2005. Crude oil emulsions: A state-of-art review. *SPE Prod. Facil.* 20, 5-13.
- Kolmogorov, A.N., 1949. On the breakage of drops in a turbulent flow. *Dokl. Akad. Nauk. S.S.S.R.* 66, 825-828.
- Kumar, M.S., Bellettre, J., Tazerout, M., 2009. The use of biofuel emulsions as fuel for diesel engines: a review. *Proc. ImechE, Part A: J. Power and Energy* 223, 729-742.
- Lemenand, T., Della Valle, D., Zellouf, Y., Peerhossaini, H., 2003. Droplets formation in turbulent mixing of two immiscible fluids in a new type of static mixer. *Int. J. Multiphase Flow* 29, 813-840.
- Lemenand, T., Habchi, C., Della Valle, D., Bellettre, J., Peerhossaini, H., 2014. Mass Transfer and emulsification by chaotic advection. *Int. J. Heat Mass Transf.* 71, 228-235.

- Lin, S., 2004. *Phys. Rev. Lett.* 92, 054503.
- Mahajan, A.J., Kirwan, D. J., 1996. Micromixing effects in a two-impinging-jets precipitator. *AIChE J.* 42, 1802-1814.
- Muijlwijk, K., Colijn, I., Harsono, H., Krebs, T., Berton-Carabin, D., Schroen, K., 2017. Coalescence of protein-stabilised emulsions studied with microfluidics. *Food Hydrocolloids.* 70, 96-104.
- Nisisako, T., Torii, T., Takahashi, T., Takizawa, Y., 2006. Synthesis of monodisperse bicolored janus particles with electrical anisotropy using a microfluidic co-flow system. *Adv. Mater.* 18, 1152-1156.
- Ohtake, T., Hano, T., Takagi, K., Nakashio, F., 1987. Effects of viscosity on drop diameter of w/o emulsion dispersed in a stirred tank. *J. Chem. Eng. JPN.* 20, 443-447.
- Perro, A., Nicolet, C., Angly, J., Lecomandoux, S., le Meins, J.F., Colin, A., 2011. Mastering a double emulsion in a simple co-flow microfluidic to generate complex polymersomes. *Langmuir* 27, 9034-9042.
- Pouton, C.W., 1997. Formation of self-emulsifying drug delivery systems. *Adv. Drug Deliv. Rev.* 25, 47-58.
- Sailim, A., Fourar, M., Pironon, J., Sausse, J., 2008. Oil-water two-phase flow in microchannels: flow patterns and pressure drop measurements. *Canadian J. Chem. Eng.* 86, 978-988.
- Schlender, M., Spengler, A., Schuchmann, H.P., 2015. High pressure emulsion formation in cylindrical coaxial orifices: Influence of cavitation induced pattern on oil drop size. *Int. J. Multiphase Flow* 74, 84-95.
- Schultz, S., Wagner, G., Urban, K., Ulrich, J., 2004. High-pressure homogenization as a process for emulsion formation. *Chem. Eng. Technol.* 27, 361-368.
- Sharp, D.H., 1983. An overview of Rayleigh-Taylor instability. Los Alamos National Lab, LA-UR-83-2130.
- Shaw, D.J., 1980, Introduction to colloid and surface chemistry. Butterworths.
- Shinnar, R., 1961. On the behavior of liquid dispersions in mixing vessels. *J. Fluid Mech.* 10, 259-275.
- Siddiqui, S.W., 2014. The effects of oils, low molecular weight emulsifiers and hydrodynamics on oil-in-water emulsification in confined impinging jet mixer. *Colloids Surf. A: Physicochemical Eng. Asp.* 443, 8-18.
- Siddiqui, S.W., Norton, I. T., 2012. Oil-in-water emulsification using confined impinging jets. *J. Colloid Interface Sci.* 337, 213-221.
- Siddiqui, S.W., Zhao, Y., Kukukova, A., Kresta, S.M., 2009. Characteristics of a confined impinging jet reactor: energy dissipation, homogeneous and heterogeneous reaction products, and effect of unequal flow. *Ind. Eng. Chem. Res.* 48, 7945-7958.
- Sprow, F.B., 1967. Distribution of droplet sizes produced in turbulent liquid-liquid dispersion. *Chem. Eng. Sci.* 22, 435-442.
- Tamir, A., 1994. *Impinging Stream Reactors.* Elsevier.
- Tamir, A., Sobhi, S., 1985. A new two-impinging-streams emulsifier. *AIChE J.* 31, 2089-2092.
- Taylor, G.I., 1932. The viscosity of a fluid containing small drops of another fluid. *Proc. Roy. Soc.* 138, 41-48.
- Theron, F., Sauze, N.L., 2011. Comparison between three static mixers for emulsification in turbulent flow. *Int. J. Multiphase Flow* 37, 488-500.
- Thorsen, T., Roberts, R.W., Arnold, F.H., Quake, S.R., 2001. Dynamic pattern formation in a vesicle-generating microfluidic device. *Phys. Rev. Lett.* 86, 4163-4166.
- Tice, J., Lyon, A., Ismaglov, R., 2004. Effects of viscosity on droplet deformation and mixing in microfluidic channels. *Anal. Chim. Acta.* 507, 73-77.
- Tsaoulidis, D., Angeli, P. 2017. Liquid-liquid dispersions in intensified impinging-jets cells. *Chem. Eng. Sci.* 171, 149-159.
- Vankova, N., Tcholakova, S., Denkov, N.D., Ivanov, I.B., Vulchev, V.D., Danner, T., 2007. Emulsification in turbulent flow 1. Mean and maximum drop diameters in inertial and viscous regimes. *J. Colloid Interface Sci.* 312, 363-380.
- Walstra, P., 1993. Principles of emulsion formation. *Chem. Eng. Sci.* 48, 333-349.
- Wegmann, A., von Rohr, P.R., 2006. Two phase liquid-liquid flows in pipes of small diameters. *Int. J. Multiphase Flow* 32, 1017-1028.
- Zhao, C.X., Middelberg, A.P.J., 2011. Two-phase microfluidic flows. *Chem. Eng. Sci.* 66, 1394-1411.